Average current mode control for GaN-based single-phase 2-level DAB converter

Giuseppe GALIOTO[1], Antonino SFERLAZZA[1], Giuseppe Costantino GIACONIA[1], Hugo MOREAU[2], Bruno ESTIBALS[2], Corinne ALONSO[2]

[1]University of Palermo, Department of Engineering, Palermo, Italy
[2]Laboratory LAAS-CNRS, Toulouse, France

ABSTRACT – Dual Active Bridge (DAB) converters are widely employed in electric vehicles charging equipment, both in Onboard Chargers (OBCs) and offboard charging infrastructure, either in Grid-to-Vehicle (G2V) or Vehicle-to-Grid (V2G) power flow. However, due to the unavoidable mismatches in device parameters, a DC bias current can bring the transformer core to saturation, compromising the converter performance. Developing a means with a dedicated current control to eliminate the parasite DC current part is therefore essential for the structure to avoid operating points in magnetic saturated regions. This work aims, through MATLAB/Simulink simulations, to design a current mode control law with its low steady-state error reducing the DC parasite current. Operating in high switching frequency, GaN or SiC devices could represent today the best option available on the market for enhancing power density, efficiency and dynamic performance of the converter.

Keywords — Average Current Control, DC bias cancellation, Dual Active Bridge (DAB), GaN components, High Switching Frequency, Magnetic Saturation Management

1. INTRODUCTION

Growing concerns about environmental issues and the demand for clean energy are driving the widespread adoption of electric vehicles (EVs). The market offers various of Battery Electric Vehicles (BEVs), each differing in charging time and driving range. While EVs are more eco-friendly and cost-effective than internal combustion engine (ICE) vehicles, challenges such as long charging times and range restrictions continue to limit their mass adoption [1].

In recent years, various isolated bidirectional DC-DC converters have been explored and proposed to enhance EV charging systems. Key design objectives for power electronics in these systems include improving efficiency, achieving high power density, and reducing overall converter costs. High-power, high-voltage EV charging systems are actively researched to significantly reduce charging time [2].

DC-DC converters come in various topologies, selected based on their power density requirements. For applications requiring bidirectional power flow, galvanic isolation, and soft-switching, the dual active bridge (DAB) converter is a preferred topology due to its multiple advantages. In fact, the DAB converter can exploit the phase shift modulation and so its simplicity: only a single control variable, the phase shift angle ϕ, is required to adjust the DAB power level. The simplicity of this modulation method and the possibility of using half bridge circuits to generate the high frequency transformer voltages are the main reasons for the wide use of this modulation method. Disadvantages are a limited operating range with low switching losses and large RMS currents in the high frequency transformer for most operating points when the DAB is operated in wide voltage ranges [3]. In terms of current stress, single-phase-shift (SPS) modulation is effective only when the voltage gain is unity. In contrast, dual-phase-shift (DPS) control [4] offers greater flexibility in power regulation, reduces reactive power, and provides two degrees of freedom through inner and outer phase shift ratios. However, different phase shift selections lead to variations in peak inductor current. Since battery voltage fluctuates throughout the charging cycle, mismatches between primary and secondary voltages cause increased inductor current peaks [5].

Also, traditional control approaches such as Single Phase Shift (SPS) and Dual Phase Shift (DPS) are the most commonly used control strategies in DAB converters. These approaches are straightforward and work well under high-load conditions. However, at light or no load, they can cause an imbalance in the average voltage across the transformer, leading to a net DC bias. This imbalance often goes unaddressed in these methods, increasing the risk of transformer core saturation due to the buildup of magnetic flux.

In practice, a DC magnetic flux bias will arise both in steady state and transient process for a DAB converter. This steady state DC bias part is caused by unmatched parameters of the circuit, such as small discrepancy of the gate-drive signal, different turn on/off delay, and unequal ON-state resistance of the power devices, while the transient DC bias one is caused by the temporary voltage-second imbalance on inductor due to the update of phase shift ratio. The steady-state DC bias will increase the conduction losses of the transformer and power devices, which leads to loss of zero voltage switching (ZVS), while the transient DC bias may saturate the magnetic cores of the transformer and inductor, leading to the failure of the converter in the end [6, 7].

Also, advanced techniques such as Model Predictive Control (MPC) [8] and adaptive control [9] have been proposed in literature. Both solutions, although with enhanced performance, present an high comupational complexity and burden for the controller. This work propose a straightforward and low complexity implementation of a double loop controller with PI regulators and analyze its performance in terms of dynamics, robustness against input/ouput variations and effectiveness in maintaining the magnetic elements of the converter inside the linear region of the magnetization curve.

Commercially available onboard chargers (OBCs) typically consist of a two-stage structure: a power factor correction (PFC) converter to minimize harmonic distortion, followed by a DC-DC converter for output regulation and electrical isolation. Figure 1 illustrates a typical OBC architecture, including both the PFC and DC-DC stages. This work focuses on the development of a control strategy for the DC-DC stage, with an emphasis on its average current control, as well as keeping a

simple modulation strategy to reduce the computational burden of the controller.

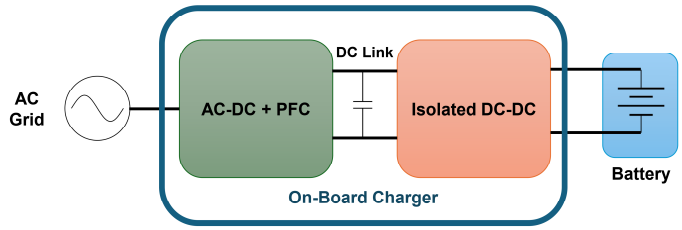

Fig. 1 On-Board Charger block diagram

2. DAB Average Current Mode Control

The basic topology of the DAB is depicted in Figure 2. There are four power GaN HEMT, forming a full bridge, on each side of the high-frequency transformer, and the transformer provides isolation between the primary and secondary sides. The equivalent inductance is represented by L_{lk}. Three different phase shift ratios can be defined respectively named D_1, D_2, D_3. D_1 acts on the phase shift between the active devices of the first half-bridge and second half-bridge on the primary side of the transformer AC Link. D_3 acts on the phase shift between the two half-bridges on the secondary side of the transformer. D_2 is the phase shift between input bridge and the output bridge, defined also as outer phase shift ratio. Through the control in magnitude and direction of the outer phase shift, the magnitude and direction of the power flow can be controlled.

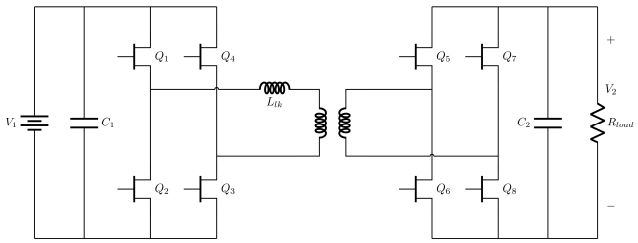

Fig. 2 GaN-based 2-Level DAB circuit diagram

The model employed to build up the controller is the reduced order model presented in [9-11]. Following its analytical deployment, the model control-to-voltage transfer function is derived as follows:

$$\frac{V_{out}}{D_2}(s) = \frac{NV_1(1-4\Phi)}{f_s L}\frac{R_L}{R_L C_2 s + 1}$$

$$\Phi = \begin{cases} 0.25 - \sqrt{\frac{1}{16} - \frac{f_s L I_2}{2NV_1}} & I_2 \geq 0 \\ -0.25 + \sqrt{\frac{1}{16} + \frac{f_s L I_2}{2NV_1}} & I_2 < 0 \end{cases}$$

$$I_2 = \frac{V_2}{R_L}$$

Where N is the transformer turns ratio, V_1 the input voltage, Φ the nominal outer phase shift, f_s the switching frequency, C_2 the output capacitor, R_L the load resistor, V_2 and I_2 the output voltage and current respectively.

The control adopts Proportional-Integral regulators thanks to their easiness of implementation, good dynamic response and low steady-state error. Following a PI implementation, the control scheme can be divided into two main loops: the voltage control loop, which, given a reference value for the output voltage, brings the error to zero thanks to a PI action on D_2 (outer phase shift ratio). The other loop starts from the measurement of the inductor current and the extraction of its average value over time (averaging time $10/f_s$). The reference value for the average inductor current is imposed to be zero and a PI action brings the error to the minimum by adjusting the duty cycle of all the gate signals of the DAB together. The control block diagram and the MATLAB/Simulink implementation are shown in Fig. 3a and 3b. In this way, the plant model is defined and the conventional PI tuning technique with the crossover frequency and phase margin constraints can be employed. This method imposes that:

$$|G_{PI}(j\bar{\omega}_t)G_{DAB}(j\bar{\omega}_t)| = 1$$

$$phase(G_{PI}(j\bar{\omega}_t)G_{DAB}(j\bar{\omega}_t)) = \left(\frac{\phi_m}{180} - 1\right)\pi$$

Where:

$$G_{PI}(j\omega) = k_p + \frac{k_i}{(j\omega)}$$

ϕ_m represent the phase margin (in degrees) and $\bar{\omega}_t$ represents the desired crossover frequency.. The procedure consists in imposing the desired crossover frequency for the closed loop system and the desired phase margin. Then the two previous equations, when solved, directly give the values of k_p and k_i to satisfy the required constraints. In this way, the PI gains can be set for the DAB model considered here.

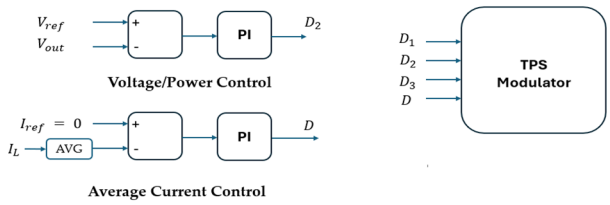

Fig. 3a Average Current Mode Control block diagram

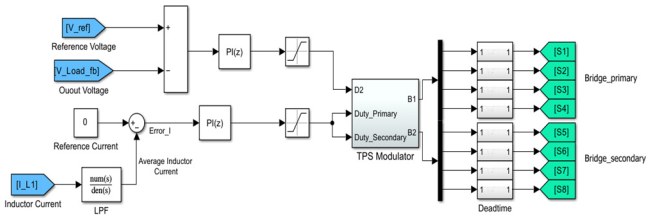

Fig. 3b MATLAB/Simulink control scheme block diagram

The modulation technique employed in this work is a Triple-Phase-Shift (TPS) modulation, which gives more control degrees of freedom to obtain the desired performance. However, a slight modification is made on the conventional TPS modulator. In fact, the duty cycles of the gate signals are also controlled, rather than just the phase shift ratios D_1, D_2 and D_3.

3. Transformer Magnetic Saturation Model

In order to validate the control algorithm, a suitable model for the transformer saturation phenomenon has to be considered. Specifically, in the following simulations an E-Core 3C95 ferrite transformer was considered and implemented through a Configurable Subsystem component. It can be configured as an ideal transformer for speeding up the simulation or as a more detailed transformer model that includes saturation behavior. For the detailed version, E65/32/27 from TDK transformer is modeled using the PLECS magnetic domain. The parameters of

the magnetic model are directly related to the geometry and material characteristics of the core, which in most cases can be obtained from datasheets. In PLECS it is then possible to obtain the B-H curve in working conditions and it is possible to verify if saturation occurs. The employed transformer parameters are presented in Table 1, while the DAB converter parameters are presented in Table 2.

Parameter	**Value**
Core Material	3C95 ferrite
Primary Turns (Np)	12 turns
Secondary Turns (Ns)	12 turns
Cross-sectional Area (Ac)	250 mm² = 2.5×10⁻⁴ m²
Effective Magnetic Path Length (le)	0.135 m
Saturation Flux Density (B_sat)	0.42 T
Saturation Field Strength (H_sat)	300 A/m (approx.)
Permeability of Free Space (μ₀)	4π × 10⁻⁷ H/m
Unsaturated Relative Permeability (μr)	2000 – 3000
Saturated Relative Permeability (μr_sat)	~10 – 20

Table 1. TDK E65/32/27 transformer parameters

Parameter	**Value**
Input voltage V_{DC}	400 V
Output voltage V_{OUT}	400 V
Maximum Output Current	16.5 A
Maximum output power P_{max}	6.6 kW
Equivalent Inductance L_{lk}	7 μH
Transformer winding ratio n	1
Input capacitance C_1	47 μF
Output capacitance C_2	47 μF
Switching frequency f_{sw}	100 kHz
Deadtime DT	100 ns

Table 2. DAB converter simulation parameters

4. SIMULATION RESULTS

The control system was simulated in PLECS™. At a first glance, the dynamic performance of the voltage loop are assessed in a double-step test with a resistive load. The simulation results of the test are shown in Fig. 4.

Different wide-spread use cases were considered to evaluate the control robustness:

- Resistive load
- Battery as active load
- Photovoltaic panels as DC source
- DC motor as dynamic load

For instance, to validate the robustness of the proposed control algorithm, a double step variation on the input voltage is imposed in the resistive load case. The main waveforms are shown in Fig. 5. As can be seen, after a first soft-start phase, a 50 V disturbance (shadowing of a Photovoltaic (PV) panel) on the input voltage is applied (blue line in Fig. 5). The green curve in Fig. 5 shows the zoomed view of the average inductor current in these working conditions, and, as can be seen, its value is well maintained below 200 mA (peak) in transient and a ±20 mA band in steady-state.

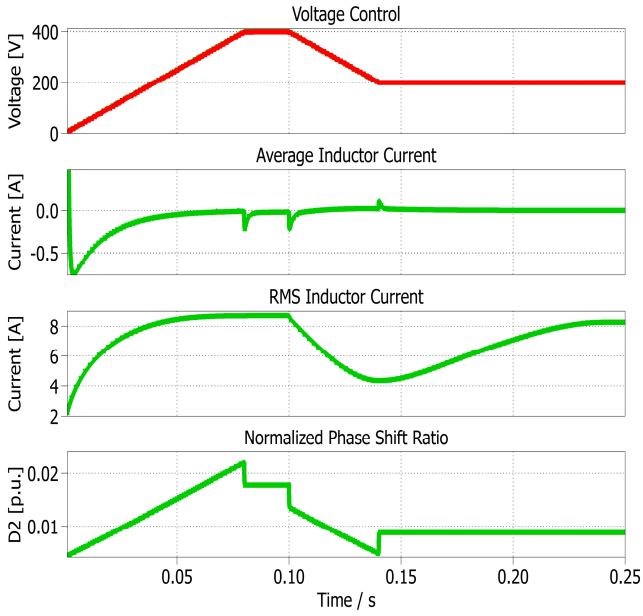

Fig. 4a Voltage control with resistive load: main waveforms for dynamic performance under double-ramp reference input

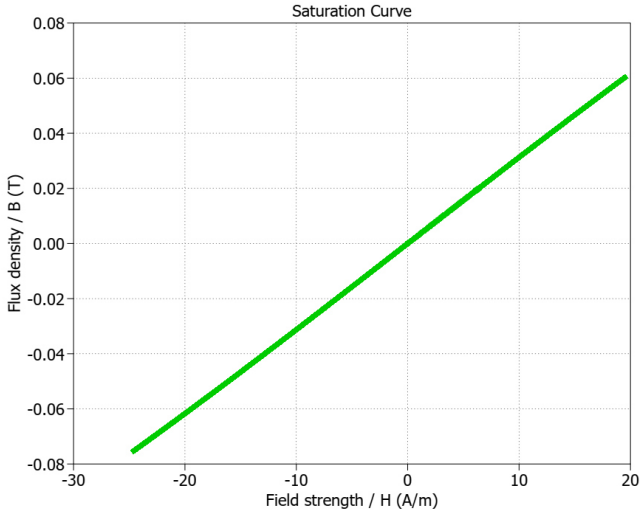

Fig. 4a B-H curve of the transformer in voltage control with resistive load during working operation under proposed control

The control algorithm has been also tested also during a charging/discharging cycle of a 400 V 10 A battery pack (112 series cells, 1 parallel branches, 1 Ah cell capacity) controlled in Constant Current (CC) / Constant Voltage (CV) mode starting from a fully discharged state. The battery parameters were scaled down, mainly in terms of current capacity, in order to reduce the simulation time. First, a pre-charge current of 3 A starts the charging process, then a constant current of 9 A charges the battery pack to the nominal voltage (400 V). As a final charging step, the battery pack is fully charged with constant voltage. Then, a discharging cycle with constant current is started until the State-of-Charge (SOC) goes back to zero. The waveforms of SOC, DAB output current, battery pack voltage and average inductor current are shown in Fig. 6. As can be seen, some the average inductor value is well maintained but also some peaks are present. However, they are very short in time and their amplitude does not affect inductor and transformer saturation (peak value well below 10 A).

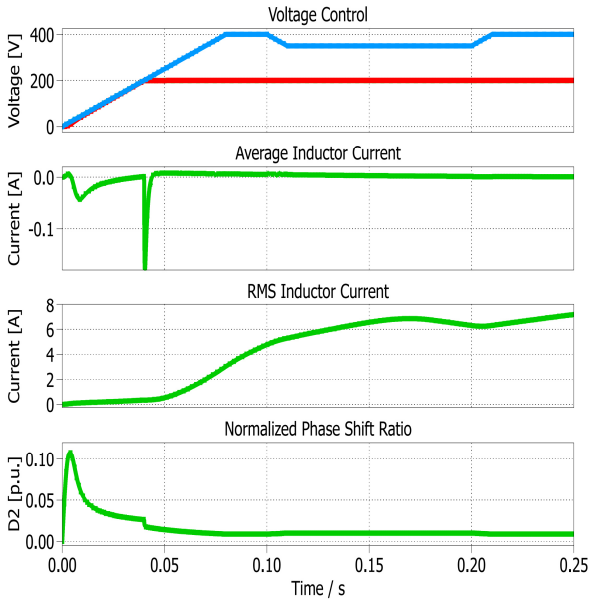

Fig. 5 Current Mode Control with resistive load: main waveforms under soft-start and distrubance in the input voltage

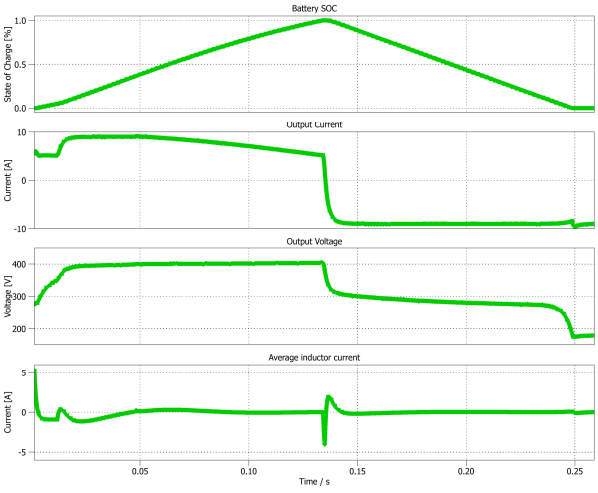

Fig. 6 Current Mode Control in battery charging/discharging: main waveforms under CC/CV charging and CC discharging

As last use-case, the driving of a DC motor is considered. A dual voltage and current loop is used to control motor speed and torque, while the external average inductor current loop is maintained to adjust the duty *D*. First, a speed step is applied to the motor (50 rad/s), and then various load steps (1,2,5 Nm) are used to assess the ability of the control to respond to dynamic load variations. As can be seen from Fig. 7, the average inductor current under control has some peaks for various load torques, but limited under ±100 mA.

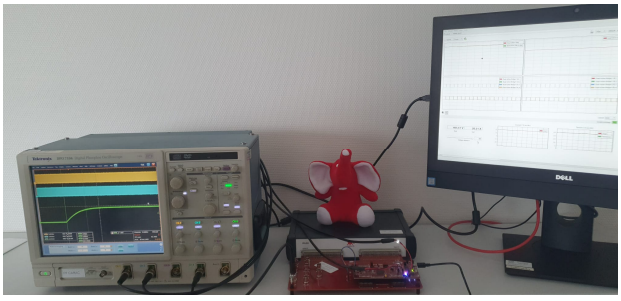

Fig. 8 Experimental testbench with Typhoon HIL 404 and TI C2000 MCU

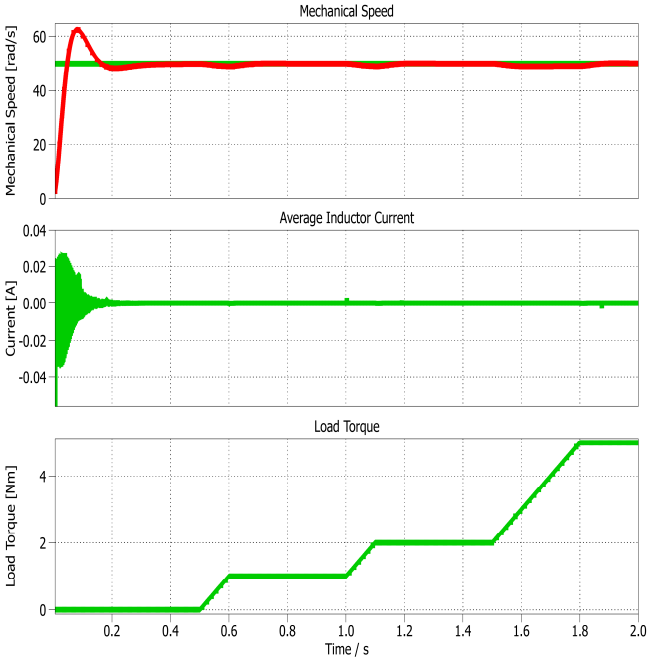

Fig. 7 Current Mode Control with DC Motor load: main waveforms under speed step and various load torques

5. Conclusions

This work has analyzed and simulated an average current mode control for a GaN-based DAB converter to avoid saturation of the inductor and transformer and all the associated detrimental effects (mainly thermal issues and lower efficiency). The control scheme has the advantage of its simple implementation and high effectiveness, which reduces the controller burden and achieves low steady-state error and a robust transient response. As a future perspective, to further validate the approach a Typhoon HIL 404 platform was employed coupled with a Texas Instruments TMS320F23879D dual-core microcontroller (MCU). The testbench is shown in Fig. 8. This choice was due to the direct compatibility between controller and emulation platform and also due to the enhanced PWM features of the C2000 line MCUs. Also, the impact of this control strategy on zero-voltage switching (ZVS) working region and efficiency must still be addressed. Also, a future work will implement the proposed control strategy in a prototype with either SiC or GaN devices. As a final remark, a parameter uncertainties analysis can be performed to assess the robustness of the proposed control scheme against parameters mismatches in devices and circuit.

6. Acknowledgements

This work has been carried out in the framework of the European Project GaN4AP (Gallium Nitride for Advanced Power Applications). The project has received funding from the Electronic Component Systems for European Leadership Joint Undertaking (ECSEL JU), under grant agreement No.101007310. This Joint Undertaking receives support from the European Union's Horizon 2020 research and innovation programme, and from Italy, France, Poland, Czech Republic, Netherlands.

7. REFERENCES

[1] J. Yuan, L. Dorn-Gomba, A. D. Callegaro, J. Reimers and A. Emadi, "A Review of Bidirectional On-Board Chargers for Electric Vehicles," in *IEEE Access*, vol. 9, pp. 51501-51518, 2021, doi: 10.1109/ACCESS.2021.3069448.

[2] Dar, A.R.; Haque, A.; Khan, M.A.; Kurukuru, V.S.B.; Mehfuz, S. "On-Board Chargers for Electric Vehicles: A Comprehensive Performance and Efficiency Review". *Energies* 2024, *17*, 4534. https://doi.org/10.3390/en17184534

[3] F. Krismer, "Modeling and Optimization of Bidirectional Dual Active Bridge DC-DC Converter Topologies*,"* Ph.D. dissertation, ETH Zurich, 2010

[4] S. Coelho, T. J. C. Sousa, V. Monteiro, L. Machado, J. L. Afonso, and C. Couto, "Comparison and Validation of Five Modulation Strategies for a Dual Active Bridge Converter ", *EAI Endorsed Trans Energy Web*, vol. 9, no. 6, p. e2, Feb. 2023.

[5] S. Shao *et al*., "Modeling and Advanced Control of Dual-Active-Bridge DC–DC Converters: A Review," in *IEEE Transactions on Power Electronics*, vol. 37, no. 2, pp. 1524-1547, Feb. 2022, doi: 10.1109/TPEL.2021.3108157.

[6] B. Zhang, S. Shao, L. Chen, X. Wu and J. Zhang, "Steady-State and Transient DC Magnetic Flux Bias Suppression Methods for a Dual Active Bridge Converter," in *IEEE Journal of Emerging and Selected Topics in Power Electronics*, vol. 9, no. 1, pp. 744-753, Feb. 2021, doi: 10.1109/JESTPE.2019.2947299.

[7] B. Zhao, Q. Song, W. Liu and Y. Zhao, "Transient DC Bias and Current Impact Effects of High-Frequency-Isolated Bidirectional DC–DC Converter in Practice," in *IEEE Transactions on Power Electronics*, vol. 31, no. 4, pp. 3203-3216, April 2016, doi: 10.1109/TPEL.2015.2445831

[8] Gao, G., Lei, W., Cui, Y., Li, K., Shi, L., & Yin, S. (2019). Modeling and Stability Analysis of Model Predictive Control Dual Active Bridge Converter. *Energies*, 12(16), 3103. https://doi.org/10.3390/en12163103

[9] Wang, X., Wang, D., Sun, G., Ni, Y., Song, K., & Li, Y. (2023). A robust voltage control of dual active full bridge converter based on RBF neural network sliding mode control with reduced order modeling approach. *Frontiers in Energy Research*, 11, 1225269. https://doi.org/10.3389/fenrg.2023.1225269

[10] A. R. Alonso, J. Sebastian, D. G. Lamar, M. M. Hernando, andA. Vazquez, "An overall study of a dual active bridge for bidirectional dc/dc conversion," in 2010 IEEE Energy Conversion Congress and Exposition, Sept 2010, pp. 1129–1135.

[11] H. Bai, C. Mi, C. Wang, and S. Gargies, "The dynamic model and hybrid phase-shift control of a dual-active-bridge converter," in 2008 34th Annual Conference of IEEE Industrial Electronics, Nov 2008, pp. 2840–2845.

[12] H. Bai, Z. Nie, and C. C. Mi, "Experimental comparison of traditional phase-shift, dual-phase-shift, and model-based control of isolated bidi rectional dc-dc converters," IEEE Transactions on Power Electronics, vol. 25, no. 6, pp. 1444–1449, June 2010.